Synchrotron X-ray transmission measurements and modeling of filters investigated for Athena

Elena Puccio[a,b,*], Michela Todaro[a,b], Ugo Lo Cicero[b,a] , Luisa Sciortino[a,b], Philippe Laurent[c], Philippe Ferrando[c], Angelo Giglia[d], Stefano Nannarone[d], and Marco Barbera[a,b]

[a] Università degli studi di Palermo – Dipartimento di Fisica e Chimica – Emilio Segrè (Palermo, Italy)
[b] INAF - Osservatorio Astronomico di Palermo Giuseppe S. Vaiana (Palermo, Italy)
[c] AIM, CEA, CNRS, Université Paris-Saclay, Université Paris (F-91191 Gif-sur-Yvette, France)
[d] Consiglio Nazionale delle Ricerche-Istituto Officina dei Materiali (CNR-IOM), 34149 (Trieste, Italy)

Abstract. Athena is a Large-class astrophysics space mission selected by ESA to study the theme "hot and energetic Universe". The mission essentially consists of a large effective area X-ray telescope and two detectors: the X-ray Integral Field Unit and the Wide Field Imager. Both instruments require filters to shield from out-of-band radiation while providing high transparency to X-rays. The mission is presently in phase B, thus, in order to consolidate the preliminary design, investigated filter materials need to be properly characterized by experimental test campaigns. In this paper, we report results from high-resolution X-ray transmission measurements performed using different synchrotron radiation beamlines, to assess the filter calibration accuracy and mitigate the risk related to selecting a unique calibration facility. The main goals of these test campaigns are: (i) verify the compliance of the investigated filter design to the scientific requirements, (ii) develop an accurate X-ray transmission model, and (iii) start identifying suitable measurement facilities and achievable accuracy for the flight filters calibration program. In particular, the X-ray transmission model of X-IFU and WFI filters has been refined within the edges of Al, C, N and O, by deriving the optical constants from two reference samples measured by synchrotron light. The achievable filter calibration accuracy has been estimated by evaluating the agreement between the best fit according to the developed transmission model and the experimental data.

Keywords: X-ray transmission, astrophysics space mission Athena, X-IFU, WFI, optical and thermal filters.

***First Author, e-mail: elena.puccio@inaf.it

1 Introduction

In the Cosmic Vision 2015-2025 Science program of ESA (European Space Agency), Athena (Advanced Telescope for High-Energy Astrophysics) has been selected as a Large-class astrophysics mission to study the dynamical, physical, and chemical properties of hot plasma in the Universe and to understand the role of black holes in shaping the environment, from local accretion disks to galaxy cluster scales[1]. The mission, with launch scheduled in 2033, is presently in phase B, ending with the Mission Adoption Review by ESA at the end of 2021.

Athena will be equipped with a large effective area (~ 1.5 m^2 at 1 keV) grazing incidence X-ray telescope with a focal length of 12 m and two interchangeable focal plane detectors: the X-ray

Integral Field Unit (X-IFU)[2], a microcalorimeter made of a hexagonal array of molybdenum-gold transition edge sensors[3], and the Wide Field Imager (WFI)[4], a large array of depleted field effect transistors (DEPFET) active pixels. The X-IFU is a cryogenic X-ray spectrometer operating at a temperature of about 50 mK in the 0.2-12 keV energy range to offer high spectral resolution (2.5 eV FWHM at 7 keV) over a field of view of 5 arcmin equivalent diameter. The WFI instrument is based on an array of silicon detectors covering a field of view of 40×40 arcmin^2 with a small detector of the same type, featuring high count rate capability, to observe very bright point sources in the 0.2-15 keV energy range over a wide field.

Both instruments require filters to attenuate out-of-band radiation, similar to optical and thermal filters already used for other instruments, such as the HRC[5] and ACIS[6] detectors on Chandra[7] and the SXS microcalorimeter on ASTRO-H (Hitomi)[8,9]. Indeed, the X-IFU detector must be shielded from incoming UV-Vis-IR radiation, due to both the optical load from bright UV-Vis astrophysical sources (e.g., massive stars, AGN's) and the IR radiation heat load from the instrument, which would degrade its energy resolution due to photon shot noise[10-12]. The X-IFU filters are each to be mounted on one of five thermal shields at the operating temperatures of 300K, 100K, 30K, 2K and 0.05K, thus becoming an integral part of the thermal engineering of the cryostat. Likewise, the DEPFET active pixel sensors of the WFI[13] are sensitive to UV-Vis photons with energies above the Si bandgap (~ 1.1 eV).

The comprehensive filter stack in the X-IFU instrument should allow an X-ray transmission compliant with the Q.E. (Quantum Efficiency) requirements[14] in Table 1. Transmission requirements[15] are derived from the Q.E. for the whole X-IFU instrument, which is given by the product of the filter stack transmission and the detector quantum efficiency. Since the X-IFU

Q.E. at low energy mostly depend on filter transmission, a filter must be extremely thin, while still compliant with both out-of-band radiation attenuation and mechanical requirements.

Before launch, both onboard instruments must be calibrated. The resolution of X-IFU is expected to be ~ 2.5 eV FWHM, thus, during calibration, the photoelectric absorption edge structure should be resolved by a factor ~10 better than the resolution required, with an absolute energy knowledge better than 0.4 eV. The calibration accuracy on the total X-IFU Q.E. (filters and detector), currently identified in the calibration plan[16], is the lowest between 4% absolute (0.04) in a given energy bin and 3% relative to the transmission in that bin, over the full energy range of interest, or a fixed value of 0.01 when Q.E. is less than 0.33. Calibration accuracy within edges is required to be 3% on ground. However, the allocation budget on calibration accuracy between the subsystems, namely, filters and detector, is yet to be defined, it is assumed to be mostly allocated to the filter full stack at lower energies, where their Q. E. is lowest and the detector one is highest, whereas the opposite is true on the higher end of the energy range. Calibration of single filters can be performed, and the requirement is met by the square sum of all filters calibration accuracies.

Given such demanding calibration requirements, we have started, as part of the research activities for the design and development of Athena X-IFU thermal filters and WFI optical filters, a campaign of X-ray transmission measurements on a set of representative filter samples made of a thin layer of polyimide coated with aluminum, using different synchrotron radiation facilities. Filter materials are chosen with a low atomic number Z, to have a high transmission in the energy band of interest while shielding the IR and NIR energy ranges (polyimide), whereas the aluminum coating has the ulterior purpose of reflecting the UV/VIS part of the spectrum. Prior work was carried out on the calibration of aluminized polyimide films to be used as filters

for previous X-ray astronomy missions[17, 18, 19]. The main goals of this campaign are: to verify the compliance of the baseline filter design to the scientific requirements, to develop an accurate X-ray transmission model for the filters, especially within element absorption edges and to start identifying suitable measurement facilities.

2 Materials and methods

2.1 Measured samples

Samples, produced by LUXEL (USA), are made of a polyimide (PI: $C_{22}H_{10}N_2O_4$) layer of either ~ 45 nm or ~ 150 nm, coated with a thin aluminum (Al) layer of either ~ 20 or ~ 30 nm. Samples with a thin PI layer are representative of the baseline for thermal filters inside the detector cooling system for the X-IFU instrument, whereas those with a thick PI layer are investigated as the baseline for the optical blocking filter of the WFI instrument.

Henceforth, all samples will be denoted by the following label: Al thickness/PI thickness in nanometers (e.g. 20/45 or 30/150). Filters are baselined to be further equipped with a honeycomb Au/Ag plated stainless steel (SS) or Nb mesh with a 5 mm pitch between cells, cell bars 50-90 µm wide and a total blocking factor of about 2% (see Fig. 1a for a filter prototype). The mesh serves multiple purposes, such as: structural strength, vibrational rigidity and improved thermal conductivity. However, for ease of measurement, the samples used in these campaigns are smaller, meshless versions mounted on a TF111/TF110 standard LUXEL frame (see Fig. 1b).

This choice is due to the fact that, in terms of X-ray transmission, the meshless samples can be thought of as a single cell of the full-scale filter, since the beam spot never exceeds a diameter of 1.2 mm, and is entirely contained in a 5 mm mesh cell. Design is still ongoing on mesh materials and geometrical properties. Nominal layer thicknesses and manufacturing tolerances are reported

in Table 2. Only two samples come from the same production batch, and measurements could not be repeated on the same sample in different facilities, since samples underwent several types of tests, some of which destructive, whereas synchrotron measurements span over three years.

2.2 Synchrotron facilities

Three synchrotron facilities were selected to measure the EUV-Soft X-ray transmission of samples:

- CNR-IOM BEAR beamline at Elettra (Trieste, Italy), for its capability of performing measurements at the C K edge (http://www.elettra.trieste.it/elettra-beamlines/bear.html);
- PTB-EUV beamline at BESSY II (Berlin, Germany), for its wide energy range including the Al K edge (https://www.ptb.de/cms/en/ptb/fachabteilungen/abt7/fb-71/ag-712.html);
- METROLOGIE beamline at SOLEIL (Univ. Paris-Saclay, France), also for its wide energy range (https://www.synchrotron-soleil.fr/en/beamlines/metrologie).

The energy ranges investigated include edges of Al, C, N and O, the elements present in each filter representative sample (see Table 3).

An edge region usually spans from ~10 eV before the edge (pre-edge) to ~50-100 eV after it (post-edge). Edge regions have to be included in the Q. E. requirements evaluation in calibration tests. Beamline measurement conditions adopted in each campaign are summarized in Table 4.

2.2.1 Transmission measurement

The experimental procedure to obtain each filter transmission is described in this section with reference to the BEAR beamline[20]. At the end of this section, relevant differences between beamline specific procedures are outlined.

The conceptual scheme of BEAR is reported in Fig. 2. The monochromator beam line is based on an entrance slitless PMPG[21] optical layout. The inclusion angle was continuously changed along the scan according to a pre-set working curve to mitigate the higher orders contributions. In addition, a suite of high-energy cut-off filters was used, including an Al filter 0.2 μm thick in the range 40-72 eV, a Si filter 0.5 μm thick in the range 72-100 eV and two Ag filters, one 0.6 μm thick in the range 250-320 eV and the other 1 μm thick in the range 1100-1600 eV.

The photon beam intensity $\Phi(\hbar\omega)$, both impinging and transmitted, were measured by an SXUV-100 photodiode. The reduction of incident photons per seconds was accomplished according to

$$\Phi(\hbar\omega) = I(\hbar\omega)/[e \cdot f(\hbar\omega)]\,, \qquad (1)$$

where $I(\hbar\omega)$ is the pico-ammeter current (I_S and I_0 for transmitted and impinging photon beam), e is the electron charge and $f(\hbar\omega)$ is the diode quantum efficiency.

The I_S and I_0 currents were measured in two separate runs (acquisition times t_1 and t_2). The I_0 signal was acquired removing the sample (sample in/out in Fig. 2) from the measuring position.

The transmission (T) was obtained according to

$$T(\hbar\omega) = \frac{I_S(\mathrm{t1}) - I_{Sd}(\mathrm{t3})}{I_{Sm}(t1) - I_{Smd}(t3)} \cdot \frac{I_{0m}(\mathrm{t2}) - I_{0md(t4)}}{I_0(\mathrm{t2}) - I_{0d}(t4)}, \qquad (2)$$

where the currents with the m subscript indicate the simultaneous monitor signals of the transmitted/impinging beam, that is, the emission current of the refocusing mirror (REFO in Fig. 2) or beam position monitoring (BPM) drain current (see Fig. 2) used in the regions of low impinging intensity (typically the C K-edge). Monitor signals allow to normalize I_S and I_0, taking into account any impinging flux variation with time, mainly due to synchrotron beam decay (Elettra works in top-up mode, typically percent over hours), together with any beam fluctuation due to beam steering.

The *d* subscripts in Eq. 2 indicate dark currents from reading pico-Ammeters. The consequent correction is crucial at the low intensity regions, especially in the C K edge region, where optics reflection is reduced by carbon contamination of optical surfaces. A schematic of the BEAR beamline setup is reported in Fig. 2.

A similar procedural scheme was adopted at Metrologie and PTB-EUV, with their particular instrumentation solutions and setups[22-24]. The light spot at sample and energy step for all beamlines are reported in Table 4. The C K edge was not acquired at PTB-EUV, and I_0 signal was recorded before and after each Is signal and averaged out, whereas at Metrologie no correction for dark current was implemented, a fact negatively affecting the signal to noise ratio in low intensity regions such as the C K edge.

3 Quantitative modeling of filter transmission

In this section, a numerical modeling of a filter transmission is presented, together with a method for recovering optical cross sections from experimental data. The model achievable accuracy in predicting filter transmission over the energy range of interest is assessed, which is important to plan the calibration activity of the flight filters.

A filter is a multi-layer of thin films, differing for thickness, atomic species and relative concentration, its transmission curve can be divided in two regions: outside and inside edges. Reliable literature values of the optical constants can be found for outside edge regions[25], however, this is not the case inside edge regions. Thus, the optical constants within edges were obtained from experimental data, after fitting outside element edges using a model of the filter transmission. The filter is described as a stack of thin films made of three materials: aluminum, polyimide, and aluminum oxide. A layer of native aluminum oxide is introduced, since its presence is known from the literature[26-28], with a stoichiometry Al_2O_3 assumed henceforth.

The filter transmission *T(E)* can be approximated as the product

$$T(E) = \prod_1^n e^{[-\mu_i(E)\cdot x_i]} \quad (3)$$

where x_i is the height of the volume occupied by the i_{th} atomic specie and μ_i is its corresponding linear attenuation coefficient. The linear attenuation coefficient is proportional to the imaginary part f_2 of the atomic scattering factors.

On the basis of Eq. 3, we develop a model for filter transmission, involving directly the atomic elements without any further constraint related to the specific material, such as its density and stoichiometry (they shall however be considered afterwards to estimate each layer thickness).

The model allows to fit experimental transmission data, provided that the atomic scattering factors are known. Outside absorption edge regions, atomic scattering factors in Henke et al. 1993[25] can be used, however, within edges, we use the model to obtain *effective* values for f_2 of each element from data. Specifically, the fit function is based on the product of the transmission due to each element and has four free parameters, each element volume height in the layer:

$$T(E) = T_{Al}\, T_C\, T_N\, T_O = e^{[-\mu_{Al}(E)\cdot x_{Al}]}\ e^{[-\mu_C(E)\cdot x_C]}\ e^{[-\mu_N(E)\cdot x_N]}\ e^{[-\mu_O(E)\cdot x_O]} \quad (4)$$

In Eq. 4, we disregard H, since it has a negligible absorption in the energy range of interest.

A preliminary fit was performed outside each element edge region on two reference samples, using Henke tabulated values for f_2. Focusing on one element at a time, e.g. Al, we then modeled the transmission curve within its edge region due to all the other elements, using the preliminary best fit parameters x_i. We then divided the experimental transmission (T_{exp}) by the modeled transmission of all the other elements, given by the product $T_C \cdot T_O \cdot T_N$ in this example. The linear attenuation coefficient (μ_{Al}) can then be calculated by dividing the logarithm of this ratio by the specific element volume height obtained from the preliminary fit. The f_2 inside a specific element

edge region are proportional to these values, which are smoothed with a polynomial and interpolated over the energy range, and can be derived as in Eq. 5 (example for Al):

$$(f_2)_{Al} \propto \mu_{Al}(E) = \frac{1}{x_{Al}} \cdot \ln\left(\frac{T_{exp}}{T_C \cdot T_N \cdot T_O}\right), \quad (5)$$

These *effective* values for f_2, calculated from the experimental data, are atomic in nature, but take into account each atom local environment within the material. For instance, since Al is present both in the metallic and aluminum oxide compounds, the f_2 calculated for Al include both components. This method can be safely applied if edges of different elements do not overlap over the same energy range, as is the case for our samples. Having obtained *effective* values for f_2 inside each edge, the fit can be performed again, over the whole energy range, now including edge regions. From these best fit parameters, all layer thicknesses can be estimated, introducing two quantities *a posteriori*: material density and stoichiometry. For instance, PI thickness can be estimated from the best fit parameter of either C or N. Starting from x_N, and dividing it by the product of PI density (1.4 g/cm^3) times the nitrogen mass fraction f_N (PI molecule $C_{22}H_{10}N_2O_4$), PI thickness $x_{PI(N)}$, can be calculated as in Eq. 6:

$$x_{PI(N)} = \frac{x_N}{\rho_{PI} \cdot f_N}, \text{ with } f_N = \frac{2A_N}{22A_C + 10A_H + 2A_N + 4A_O} \quad (6)$$

In principle, the same calculation can be carried out using x_C, but oxygen cannot be used since it is also involved in aluminum oxide. However, knowing the PI layer thickness from N, the Al_2O_3 layer thickness can be derived from the remaining number density of O atoms.

Finally, to define a 3σ confidence interval (CI) and assess the accuracy achievable by the transmission model, the percent relative error *(%err*) between best fit and data was calculated and the corresponding CI estimated by modeling the maximum and minimum fit curves according to the best fit.

4 Results and Discussion

Experimental transmission data are shown in Fig. 3 for thin samples (X-IFU thermal filters) and in Fig. 4 for thick samples (WFI optical blocking filters), comparing results obtained at different beamlines. Notice that samples PN 3203 measured at Elettra and PN 3204 measured at SOLEIL come from the same batch and thus the corresponding transmission data are closer, whereas sample PN 2472 has slightly less Al (see Al L edge in Fig. 2). The opposite is true for the thick samples, where sample PN 2460 measured at BESSY shows a slightly thicker coating of Al.

In Fig. 5, the fit performed outside edge regions using tabulated scattering factor is plotted, for a reference filter (PN 3096). The experimental data of this filter was used to obtain the *effective* values for f_2 of elements C, N and O in the ranges: 280 eV-375 eV, 395 eV-450 eV and 527 eV-570 eV. A different reference filter (PN 2460) was used to obtain *effective* values for f_2 of Al inside its L and K edges: 72 eV-220 eV and 1550 eV-1670 eV.

After obtaining the *effective* values for f_2 in all the elements edge regions from the reference samples, a best fit was performed for all the samples, now including edges, to find each layer thickness (see Table 5, where a star indicates reference samples).

From Table 5, the sum of Al and Al_2O_3 thickness is just a few nm less than the nominal value provided by the filter manufacturer. This remains true when comparing the equivalent Al amount (equiv. Al in Table 5), calculated from the total number of Al absorbers divided by the Al density 2.7 g/cm^3. Possibly, the actual Al coating density could be slightly lower than expected, because of the nanometric scale of the layer and the technological process involved. The Al_2O_3 thickness is in line with what is expected if the spontaneous oxidation process occurred on both surfaces of the Al layer, since the value found in the literature is 3-4 nm per surface[26]. A slight variability in Al_2O_3 thickness is observed, probably due to different ages of the samples, ranging

from a few months to four years old. The thickness of the PI layer estimated from N is in overall good agreement with the nominal thickness, except for the reference sample where it is underestimated. The authors have no clear explanation about this slight discrepancy, possibly the fact that this sample was used as the reference sample to retrieve the *effective* f_2 may have influenced the result. In any case, the PI layer thickness from C is consistently overestimated. There are at least two possible explanations: the first one is that samples, which have been exposed to air in some instances, have some C surface contamination; the second is that there is either a different stoichiometry of the PI or carbon-based molecules trapped somewhere within or between layers. We have a few X-ray Photoelectron Spectroscopy (XPS) measurements, which preliminarily indicate the presence of C surface contamination.

In Figs. 6-8, datasets of thin samples with their best fit are shown, whereas a plot with the *%err* along with its CI is plotted in Fig. 9 for a thin sample, with a red vertical line to signal the low energy threshold for the nominal sensitivity of the Athena X-ray sensors (200 eV), and two horizontal lines to display the filter calibration requirement of ±1% relative error.

Data at E < 200 eV, where the sample has a lower transmittance, are still important to accurately estimate the Al layer, since the L edge is very sensitive to changes in the number of Al absorbers. The best fit is overall in good agreement with all datasets, even inside edge regions. Regarding BESSY II and SOLEIL, the agreement of the fit to the data is very good, with a percent relative error in transmission below 1% everywhere, except in the C, N, and O K-edges, where *effective* f_2 were obtained from the thick sample measured at Elettra. Looking at the C K-edge measured at SOLEIL, the shape is noticeably different from the same edge measured at Elettra, making this measurement less reliable (as expected). The N K-edge measured at SOLEIL is also quite noisy, whereas at BESSY the energy step is one order of magnitude bigger with respect to the Elettra

one. Regarding the O K edge, the scattering factors were recovered from a thick sample, where the relative amount of O in PI with respect to Al_2O_3 is bigger, also causing a difference in edge shape between thin and thick samples as measured by all beamlines.

For what concerns Elettra, the fit is also in good agreement with the data, with a percent relative error in transmission below 1.5% in the energy range of interest for Athena, excluding the C, O and Al K-edges. Within these edges, the model reproduces the data less well, due to:

- A ~0.1 eV shift in the energy calibration of the C K-edge between thin and thick samples. Since the reference sample from which *effective* f_2 were recovered is the thick one, this shift also reflects on the fit accuracy for the thin sample in this region;
- BEAR performance at the high energy end of its range, where it is currently suffering an important contamination of beam purity ascribed to stray zero-order light coming from diffuse scattering at the grating and causing, in data reduction, an unphysical decrease of the transmission as the energy increases. Empirical numerical correction is possible and has been proven of use for spectroscopy purposes, though this fact does not make BEAR the first choice for a quantitative measurement of the transmission in this range.

The agreement between best fit and data, in terms of percent relative error, is summarized in Table 6, grouped by energy range. The N, O and Al K edges are reported separately, whereas the more problematic C K edge is not included.

Overall, the model is in good agreement with the data, in terms of percent relative error. However, some improvement is necessary to meet the X-IFU strict calibration requirements, especially within C and O K-edges, both in terms of obtaining improved *effective* f_2 and of developing an absolute energy scale calibration strategy. The *effective* f_2, however, appear well suited to model each element edge region, thus increasing the fit agreement with the data.

5 Conclusions

The two onboard instruments of the astrophysics space mission Athena, X-IFU and WFI, have severe calibration requirements. In order to meet the goals of the filters calibration plan, we have started several X-ray measurement campaigns, using different European synchrotron radiation facilities. Our aim is to characterize filter materials, presently investigated for the filters preliminary design, and to get some confidence on the measurement accuracies achievable in the flight filters calibration program. More than one facility is needed in this regard, to mitigate the risk of potential unavailability of the beamline during calibration measurements on flight filters.

Transmission data were acquired for six filter samples, made of a thin polyimide membrane coated with aluminum, at three different synchrotron facilities: CNR-IOM BEAR at Elettra (Trieste, IT), PTB-UV at BESSY II (Berlin, DE) and METROLOGIE at SOLEIL (Univ. Paris-Saclay, FR). A model was developed, based on the transmission of a gas of elements Al, C, O, N, with four free parameters, to determine each layer thickness. New *effective* values for the imaginary part of the scattering factors were obtained by a preliminary fit of two reference samples, with the goal of refining the fit accuracy within edge regions. The layer thicknesses obtained from the best fit parameters are in general in good agreement with the nominal ones.

The percent relative error between best fit and data was evaluated, to estimate the model accuracy in reproducing the data, in view of satisfying the strict calibration requirements of the X-IFU instrument. A good agreement between the measured transmission and best fit was found for all the sample filters. Finally, actions should be undertaken in acquiring more accurate data, such as developing an absolute energy calibration strategy specific for our samples, which takes into account the very strict calibration requirements of X-IFU filters, to be run prior to each experimental campaign, and investigating filter surface C contamination.

Acknowledgments

The use of CNR-IOM BEAR beamline at Elettra was possible through the acceptance of proposal n. 20170078 titled "XAS of Al/polyimide and Si_3N_4 filters for high-energy resolution detectors in astrophysical missions as ATHENA". The use of PTB-EUV beamline at BESSY II was made available by ESA within the research project "Large Area high-performance Optical Filters for X-ray instrumentation – LAOF" contract n. 4000120250/17/NL/BJ. The use of METROLOGIE beamline at SOLEIL was possible through the acceptance of proposal n. 20180061 titled "ATHENA filters transmission measures". We are grateful to Pascal Mercere and Paulo da Silva for their assistance in using the beamline. This research has received funding from ASI (Italian Space Agency) under contracts n. 2015-046-R.0 and n. 2018-1l.-HH.O, and from EU Horizon 2020 Program under the AHEAD project, grant agreement n. 654215. We acknowledge fruitful discussions and support by LUXEL corp.

References

1. X. Barcons et al., "Athena: the X-ray observatory to study the hot and energetic Universe", *J. Phys. Conf. Ser* **610**, 012008 (2015) https://doi.org/10.1088/1742-6596/610/1/012008.
2. D. Barret et al., "The ATHENA X-ray integral field unit (X-IFU)", *Proc. SPIE* **10699**, 106991G (2018) https://doi.org/10.1117/12.2312409.
3. S. J. Smith et al., "Transition-edge sensor array development for the ATHENA x-ray itegral field unit", *Proc. SPIE* **10699**, 106991L (2018) https://doi.org/10.1117/12.2313428.
4. N. Meidinger et al., "Development of the wide field imager instrument for ATHENA", *Proc. SPIE* **10699**, 106991F (2018) https://doi.org/10.1117/12.2310141.
5. S. S. Murray et al., "In-flight performance of the Chandra high-resolution camera", *Proc. SPIE* **4012**, 68-80 (2000) https://doi.org/10.1117/12.391591.

6. G. P. Garmire et al., "Advanced CCD imaging spectrometer (ACIS) instrument on the Chandra X-ray Observatory", *Proc. SPIE* **4851**, 28-44 (2003) https://doi.org/10.1117/12.461599.
7. M. Weisskopf et al., "Chandra X-ray Observatory Overview", *Proc. SPIE* **4012**, 2-16 (2000) https://doi.org/10.1117/12.391545.
8. T. Takahashi, et al. "Hitomi (astro-h) x-ray astronomy satellite*." J. of Astronomical Telescopes, Instruments, and Systems* **4.2**, 021402 (2018) https://doi.org/10.1117/1.JATIS.4.2.021402.
9. M. E. Eckart, et al. "Ground calibration of the Astro-H (Hitomi) soft x-ray spectrometer." *J. of Astronomical Telescopes, Instruments, and Systems* **4.2**, 021406 (2018) https://doi.org/10.1117/1.JATIS.4.2.021406.
10. M. Barbera et al., "Baseline design of the thermal blocking filters for the X-IFU detector on board ATHENA", *Proc. SPIE* **9144**, 91445U (2014) https://doi.org/10.1117/12.2057403.
11. M. Barbera et al., "Thermal Filters for the ATHENA X-IFU: ongoing activities toward the conceptual design", *J.Low Temp. Phys.* **184**, 706 (2016) https://doi.org/10.1007/s10909-016-1501-4.
12. M. Barbera et al., "ATHENA X-IFU thermal filters development status toward the end of the instrument phase-A", *Proc. SPIE*, **10699**, 106991R (2018) https://doi.org/10.1117/12.2314450.
13. M. Barbera et al., "ATHENA WFI optical blocking filters development status toward the end of the instrument phase-A", *Proc. SPIE* **10699**, 106991K (2018) https://doi.org/10.1117/12.2314448.
14. P. Peille, "X-IFU Performance Requirements Document", *XIFU-RD-SYS-00278-CNES* (2019), CNES Technical Report part of the Athena X-IFU I-PRR documentation.
15. X-IFU Instrument Team, "X-IFU Thermal Filters' Stack Requirements Document", *XIFU-RD-10000-00347-CNES* (2019), CNES Technical Report part of the Athena X-IFU I-PRR.
16. François Pajot with inputs from the X-IFU Calibration Team, "X-IFU Calibration Plan", *XIFU-PL-XCAT-180626-IRAP* (2019), IRAP Technical Report part of the Athena X-IFU I-PRR.

17. G. Chartas et al., “ACIS UV/optical blocking filter calibration at the National Synchrotron Light Source”, *Proc. SPIE* **2805**, Multilayer and Grazing Incidence X-Ray/EUV Optics III, (1996) https://doi.org/10.1117/12.245111.
18. L. K. Townsley et al., “Transmission maps of the ACIS UV/optical blocking filters”, *Proc. SPIE* **2805**, Multilayer and Grazing Incidence X-Ray/EUV Optics III, (1996) https://doi.org/10.1117/12.245086
19. R. L. Kelley et al., “The Suzaku high resolution x-ray spectrometer”, *Publications of the Astronomical Society of Japan* **59.sp1**, S77-S112 (2007) https://doi.org/10.1093/pasj/59.sp1.S77
20. S. Nannarone et al., “The BEAR beamline at Elettra”, *AIP Conference Proc.* **705**, 450 (2004) https://doi.org/10.1063/1.1757831 at http://www.Elettra.trieste.it/Elettra-beamlines/bear.html
21. G. Naletto et al., “A high resolution monochromator covering wide ultraviolet spectral ranges with a single grating”, *Pure & Applied Optics*: *Journal of the European Optical Society Part A* **1.6**, 347 (1992) https://doi.org/10.1088/0963-9659/1/6/007
22. F. Scholze et al., “New PTB beamlines for high-accuracy EUV reflectometry at BESSY II”, *Proc. SPIE* **4146,** (2000) https://doi:10.1117/12.406678.
23. R. Klein et al., “The Electron Storage Rings MLS and BESSY II as Primary Source Standards.” *mitteilungen* S: 7.
24. M. Idir et al., “Metrology and Tests beamline at SOLEIL Design and first results”, *AIP Conference Proceedings* **1234**, 485 (2010) https://doi.org/10.1063/1.3463247.
25. B.L. Henke et al., “X-Ray Interactions: Photoabsorption, Scattering, Transmission, and Reflection at E = 50-30,000 eV, Z = 1-92”, *At. Data Nucl. Data Tables* **54**, 181-342 (1993) https://doi.org/10.1006/adnd.1993.1013 data available at: http://henke.lbl.gov/optical_constants/sf/
26. L. Sciortino et al., “Surface investigation and aluminum oxide estimation on test filters for the ATHENA X-IFU and WFI detectors”, *Proc. SPIE* **9905**, 990566 (2016) https://doi.org/10.1117/12.2232376.

27. Barbera et al., Exp. Astr. 7, 51-63 (1997), https://doi.org/10.1023/A:1007919005280%20

28. Barbera et al., Proc. SPIE, 8859, 14, 1-12 (2013), https://doi.org/10.1117/12.2030896

Biographies

Elena Puccio, Master Degree in physics, obtained her Ph.D. in Physics in 2017 working on Big data, Network theory, correlation and cluster analysis. She is currently a post-doc researcher at the University of Palermo (Italy) with a three years fellowship, affiliated with INAF-OAPa, to work on the design, development, experimental characterization and modeling of optical blocking filters and thermal filters for the WFI and X-IFU instruments on board the large astrophysics mission Athena funded by ESA.

Michela Todaro is a physicist, with a Ph.D. in Material Science and Nanotechnology (2018). She won a post-doc scholarship at the Astrophysics National Institute (INAF-OAPA) in 2018, on remote sensing through aerostatic devices. She currently has a Post-Doctoral fellowship at the University of Palermo, on the experimental characterization of the spectral and morphological properties of prototype filters of the X-IFU and WFI instruments onboard the ATHENA mission of ESA.

Ugo Lo Cicero, PhD in Electronic Engineering, is a senior technologist at INAF. He works on the development of new technologies for Astrophysics, in particular related to X-ray instrumentation. He has worked on the design and development of microcalorimeter arrays, active optics, X-ray sources and on the design and extensive characterization of cryogenic X-ray

409 filters. He is System Manager for the “Thermal Filters” subsystem of the XIFU instrument on
410 board ESA flagship mission Athena.
411
412 Luisa Sciortino obtained a Ph.D. in Chemistry in 2012. She has been working on the
413 development and design of the thermal and optical blocking filters of the X-IFU and WFI
414 instruments on board the Athena mission. Her expertise is the spectroscopic characterization of
415 materials and nanomaterials. She is currently a researcher of the Department of Physics and
416 Chemistry of the Università degli Studi di Palermo.
417
418 Philippe Laurent is working at the CEA Astrophysical Department in France. He is specialized in
419 High Energy Astrophysics and got his PHD in 1992, studying Black Holes X-ray binaries high-
420 energy emission. In parallel, he developed a theoretical model of radiation transfer in the
421 environment of black holes. He participates to the ESA/INTEGRAL gamma-ray mission since
422 1995, and is now the IBIS telescope Co-PI. He is also co-chair of the ATHENA background
423 studies topical group.
424
425 Philippe Ferrando obtained a PhD in high energy astrophysics in 1987. He has been working on,
426 and was Co-I of, cosmic-rays instruments onboard HEAO3, Voyager, and Ulysses. In 1995 he
427 turned to X-rays and was responsible for the calibration team of the EPIC cameras on XMM-
428 Newton. He has been P.I. of several mission proposals and phase A studies, in particular of the
429 SIMBOL-X hard X-rays telescope. He is currently deputy-head of the CEA Astrophysics
430 Department.
431

Angelo Giglia obtained his degree in Engineering of Telecommunications in 1999 and the PHD in 2006 in Engineering of Materials and Environment. He is technologist and beamline scientist for experiments for absorption X, reflectivity and photoemission spectroscopies at the synchrotron beamline BEAR@Elettra of the CNR IOM Laboratory, from april 2002 with a permanent position. His activity consists mainly in the use of UV-soft X-rays synchrotron Light for the characterization of materials and devices.

Stefano Nannarone graduated in Physics in 1967, University Roma La Sapienza. Presently retired from the University of Modena-Reggio Emilia (professor of General Physics), associated fellow of CNR and scientific responsible of IOM-CNR synchrotron beamline BEAR (Elettra, Italy). Scientific activity covered electronic and structural properties of solids, surfaces and interfaces studied by optical (lab and synchrotron) and electron scattering techniques. Teaching experience included General and Solid state Physics, Solid state Devices and elementary Quantum Chemistry.

Marco Barbera (Ph.D. in Physics) is associate professor of Astrophysics at University of Palermo, Italy (2004). He is affiliated with INAF-OAPa with responsibilities in the operation of X-ray Astronomy Calibration and Testing facility for development/test of instrumentation for X-ray Astronomy missions (filters, optics, detectors) such as Chandra, Newton-XMM, Hinode, Chang'E-1, Coronas Photons, Athena and eXTP. He is responsible for the development of filters of the WFI and X-IFU instruments on board ESA space mission Athena.

Tables

Table 1 X-IFU Q. E. and filter transmission requirements for the comprehensive filter stack.

Energy	X-IFU Q.E.	$T_{filters}$
0.35 keV	≥ 17 %	≥ 21 %
1 keV	≥ 67 %	≥ 76 %
7 keV	≥ 72 %	≥ 89 %
9.5 keV	≥ 50 %	≥ 89 %

Table 2 Nominal layer thicknesses of Al and PI for each sample with its tolerances from the manufacturer displayed in parenthesis. Next to each sample, in parenthesis, is indicated the synchrotron facility where it was measured.

Sample (synchrotron)	Part Number (PN)	Al (nm)	PI (nm)
20/45 (Elettra)	3203	20.6 (2.5)	45.5 (5)
20/45 (SOLEIL)	3204	20.6 (2.5)	45.5 (5)
20/45 (BESSY II)	2472	21.5 (2.5)	42.7 (5)
30/150 (Elettra)	3096	31.1 (5)	149.7 (5)
30/150 (SOLEIL)	2677	28.8 (5)	153.4 (5)
30/150 (BESSY II)	2460	30.4 (5)	157.8 (5)

Table 3 Atomic L- and K-edges indicative energy ranges in the measured samples.

Element	L-edges	K-edge
Al	73 eV, 118 eV	1560 eV
C	-	284 eV
N	-	402 eV
O	-	532 eV

Table 4 Measurement parameters adopted for the campaigns at BEAR (Elettra - Trieste, IT), PTB-EUV (BESSY II - Berlin, DE), and METROLOGIE (SOLEIL - Paris, FR) beamlines.

	BEAR at Elettra	PTB-EUV at BESSY II	METROLOGIE at SOLEIL
Spot size	0.4x0.7 mm^2 (VxH)	1.2x1 mm^2 (VxH)	0.6-1x1 mm^2 (VxH)
Spectral resolution	$E/\Delta E \sim 2000$	$E/\Delta E > 1000$	$E/\Delta E > 1000$
Energy range	40-1650 eV	55-1800 eV	30-2000 eV
Energy step	0.05 eV	2-20 eV outside edge regions 0.2-0.4 eV inside edge regions	1-2 eV outside edge regions 0.2-0.5 eV inside edge regions
Number of data points	~ 32000	~ 800	~ 3000

Table 5 Layer thickness of each material (Al, Al_2O_3, and PI) with its 3σ statistical uncertainty in parenthesis, as obtained from the best fit parameters.

Best fit thicknesses (nm)						Nominal thickness (nm)	
Sample (synchrotron)	**Al**	**Al_2O_3**	**equiv. Al**	**PI (from N)**	**PI (from C)**	**Al (nm)**	**PI (nm)**
20/45 (Elettra)	9.4 (0.2)	8.5 (0.2)	16.00 (0.02)	45.5 (1.1)	57.8 (0.1)	20.6 (2.5)	45.5 (5)
20/45 (SOLEIL)	9.1 (0.6)	8.5 (0.7)	15.61 (0.06)	49 (4)	58.3 (0.5)	20.6 (2.5)	45.5 (5)
20/45 (BESSY II)	9.3 (1.0)	7.4 (1.1)	15.0 (0.1)	46 (6)	55.9 (1.1)	21.5 (2.5)	42.7 (5)
30/150 (Elettra)*	20.6 (0.2)	9.4 (0.3)	27.90 (0.03)	137.5 (1.3)	177.3 (0.2)	31.1 (5)	149.7 (5)
30/150 (SOLEIL)	18.4 (1.5)	11 (2)	26.8 (0.2)	146 (10)	178.0 (1.3)	28.8 (5)	153.4 (5)
30/150 (BESSY II)*	23 (3)	10 (4)	30.6 (0.5)	164 (20)	197 (3)	30.4 (5)	157.8 (5)

* reference samples used for the determination of the *effective* values for f_2 inside edges.

Table 6 Percent relative error between data and best fit for 20/45 samples grouped by energy range (in eV). K edges are listed separately and the C K edge is not reported.

	Percent relative error (%)					
Sample (synchrotron)	**0.2<E<0.4 keV**	**N K edge**	**0.4<E<0.6 keV**	**O K edge**	**E>0.6 keV**	**Al K edge**
20/45 (Elettra)	<±1.5	<±1	<±1	>3	<±1	<±2.7
20/45 (BESSY II)	<±1	<±1.2	<±1	>3	<±1	<±1
20/45 (SOLEIL)	<±1	<±1.7	<±1	>3	<±1	<±1

Figure Caption List

Fig. 1 Sample filters with a thin PI membrane, coated with Al. (a) Filter sample with a 5 mm pitch Au plated SS honeycomb mesh mounted on a TF130 standard frame. (b) Meshless filter sample mounted on a TF110 standard frame, as used in the campaigns here reported.

Fig. 2 Conceptual scheme of the BEAR beamline, downstream from synchrotron (Elettra) on the right (not shown): beam position monitor (BPM), polarization selector (not used, fully open in these runs), PGPM monochromator (two gratings, GNIM not used in these runs) and G1200, exit slit and filter wheel, light shutter, REFO refocusing mirror, sample stage (cooling system not used in these runs) with sample mounted and beam in/out movements in the experimental chamber (base pressure low 10^{-9} mbar) together with light detector (AXUV diode). Instruments indicate p-Ammeters measuring monitor current, sample drain current (not used in these runs) and diode current. BPM plates drain current p-Ammeters not shown in figure.

Fig. 3 Comparison between experimental transmission data acquired at Elettra (orange line), SOLEIL (blue line) and BESSY II (black line) on 20/45 thin samples. Data in the C K-edge is absent for BESSY II. Insets show zooms of edges element-wise.

Fig. 4 Comparison between experimental transmission data acquired at Elettra (orange line), SOLEIL (blue line) and BESSY II (black line) on 30/150 thick samples. Data in the C K-edge is absent for BESSY II. Insets show zooms of edges element-wise.

Fig. 5 Experimental data (black dots) of a reference thick sample measured at Elettra (PN 3096), used to obtain *effective* values of f_2 for C, N and O (red line).

Fig. 6 Dataset of 20/45 sample (black dots) measured at Elettra with its best fit (red line).

Fig. 7 Dataset of 20/45 sample (black dots) measured at SOLEIL with its best fit (red line).

Fig. 8 Dataset of 20/45 sample (black dots) measured at BESSY II with its best fit (red line).

Fig. 9 Percent error (*%err)* between data and best fit (blue squares) for sample 20/45 measured at BESSY II with its CI (grey area). Red lines define the range of interest for filter calibration.

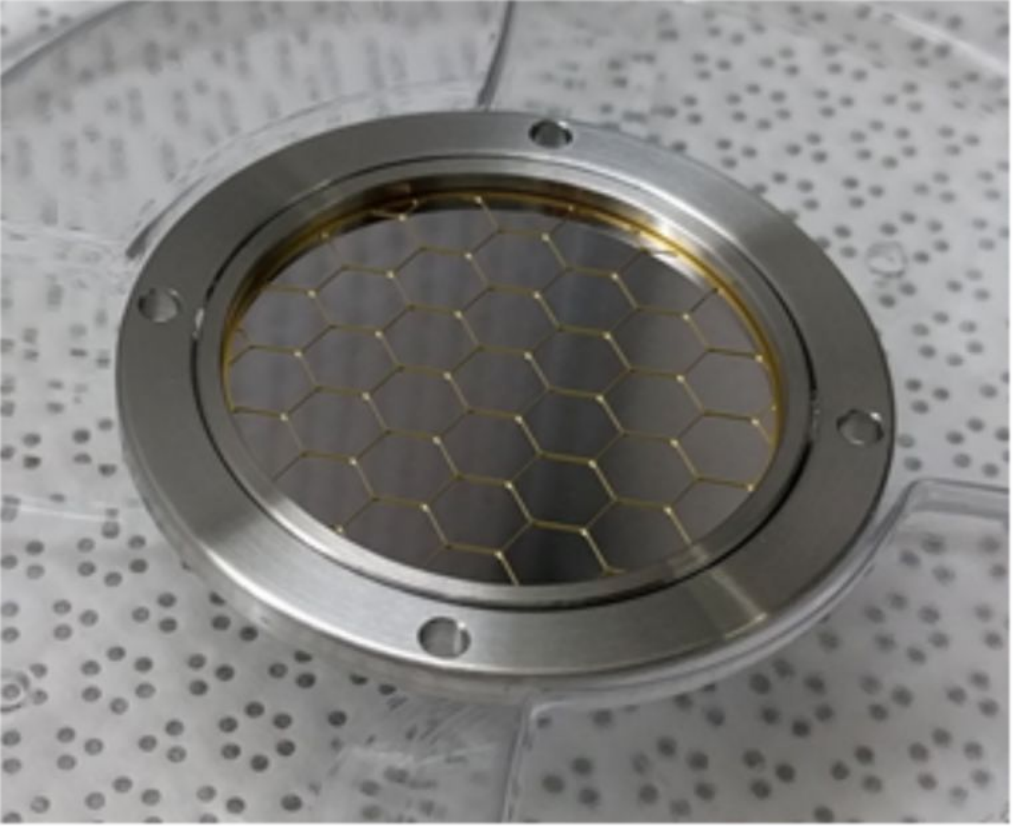

a)

b)

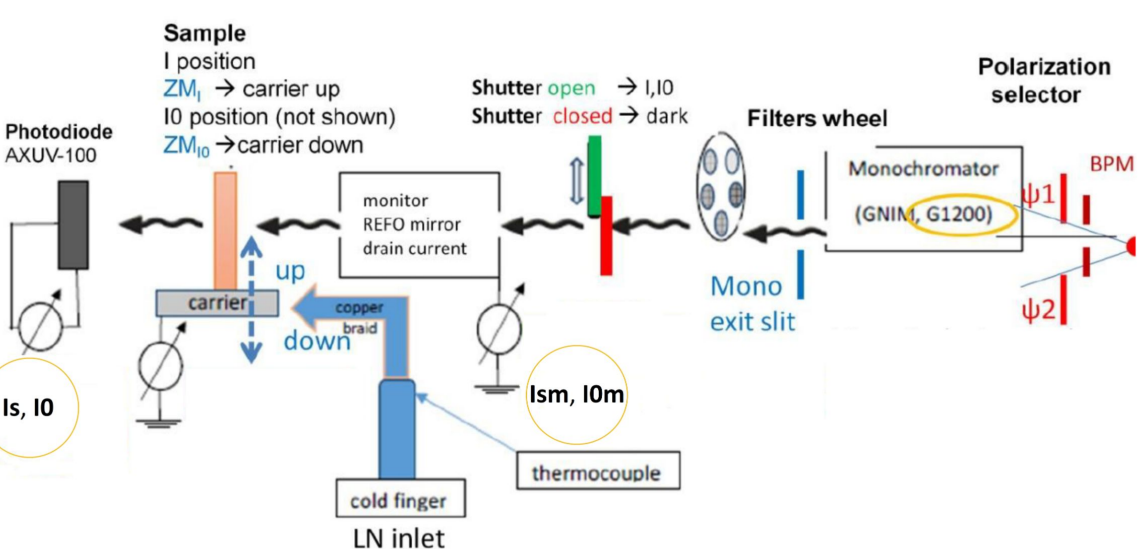
Sample
I position
ZM$_I$ → carrier up
I0 position (not shown)
ZM$_{I0}$ →carrier down
Photodiode
AXUV-100
Shutter open → I,I0
Shutter closed → dark
Filters wheel
Polarization selector
Monochromator
(GNIM, G1200)
BPM
ψ1
ψ2
monitor
REFO mirror
drain current
up
carrier
copper
braid
down
Mono
exit slit
Is, I0
Ism, I0m
thermocouple
cold finger
LN inlet

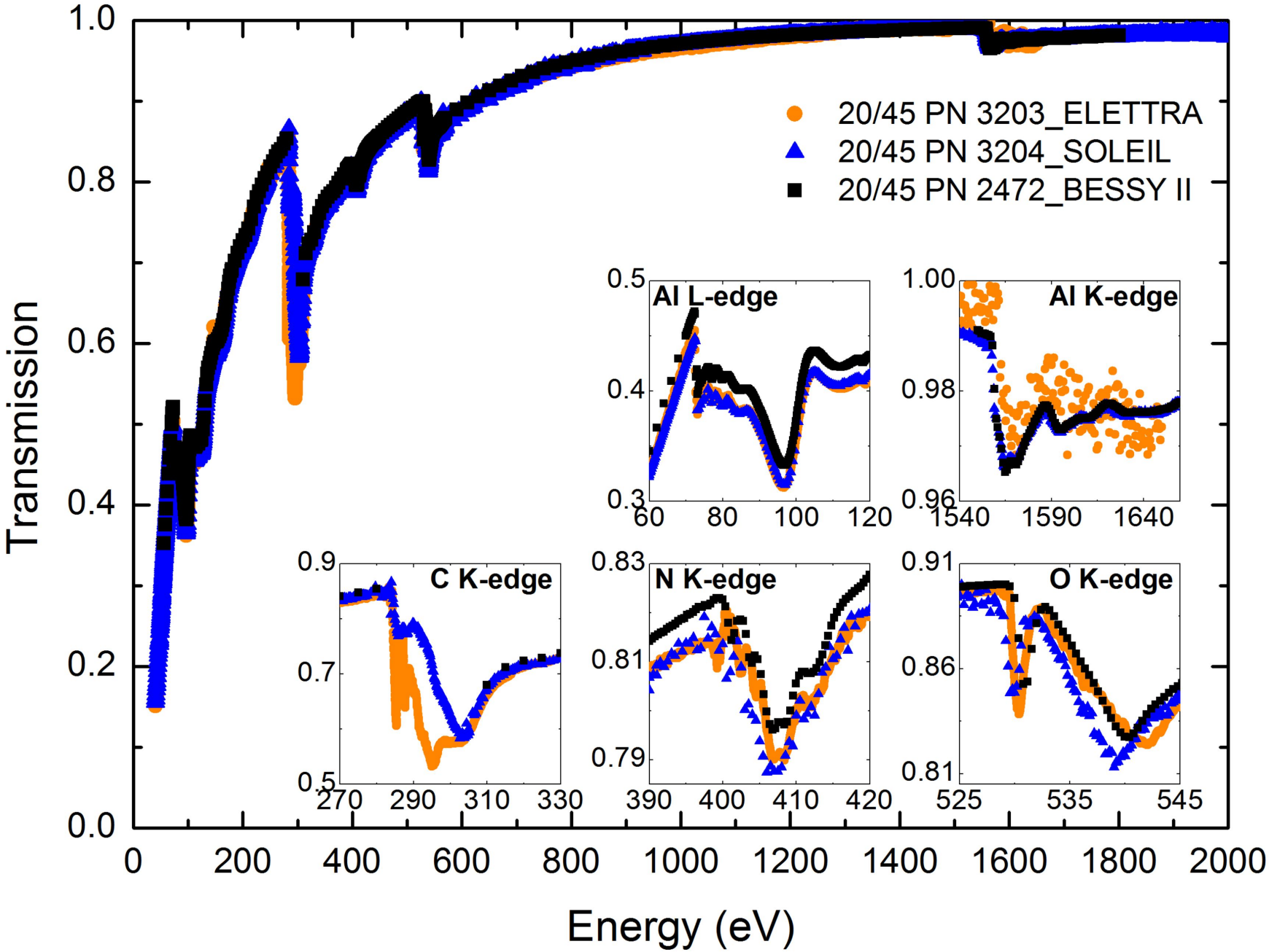
20/45 PN 3203_ELETTRA
20/45 PN 3204_SOLEIL
20/45 PN 2472_BESSY II
Transmission
Energy (eV)
Al L-edge
Al K-edge
C K-edge
N K-edge
O K-edge

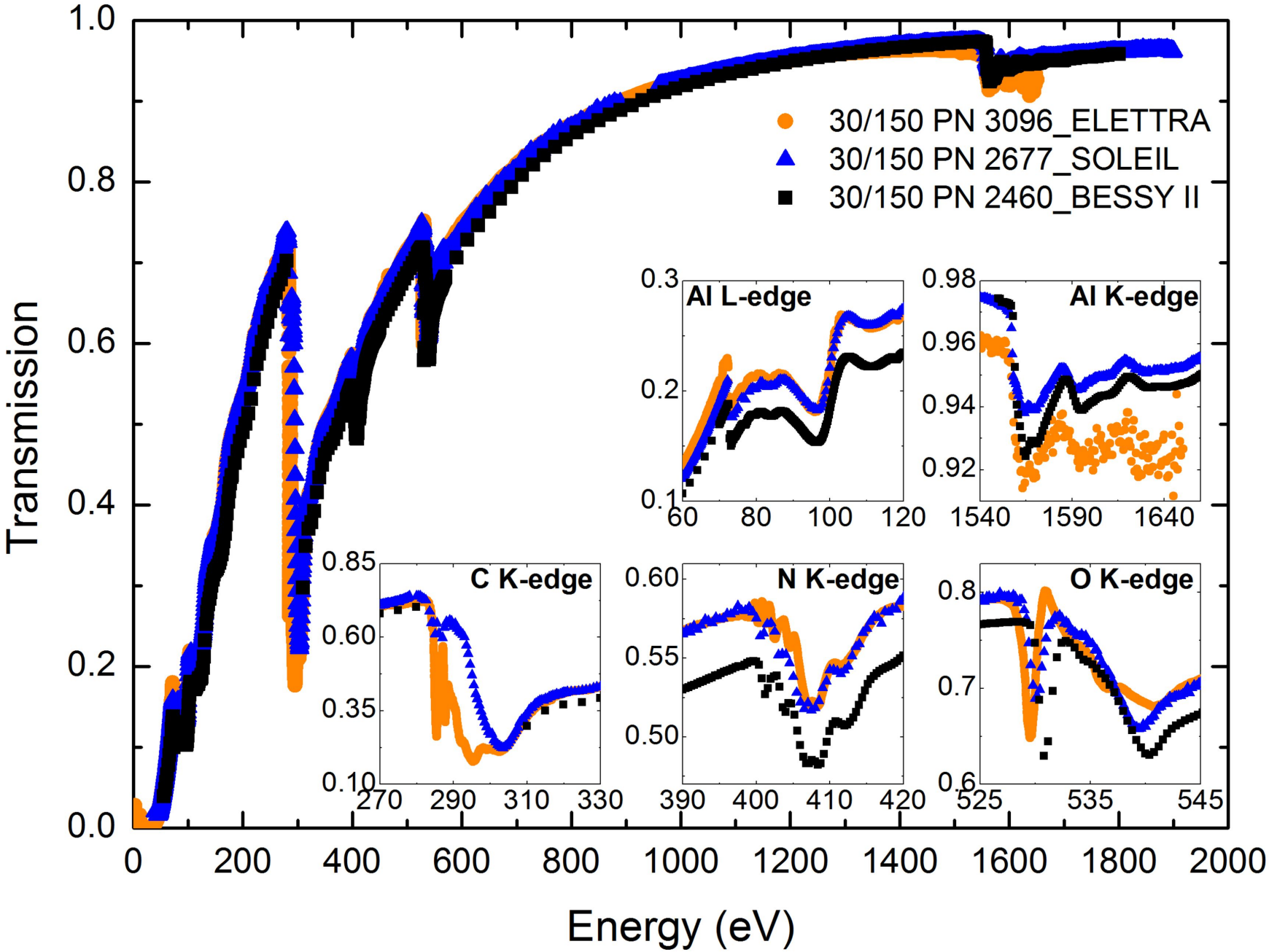
30/150 PN 3096_ELETTRA
30/150 PN 2677_SOLEIL
30/150 PN 2460_BESSY II
Transmission
Energy (eV)
Al L-edge
Al K-edge
C K-edge
N K-edge
O K-edge

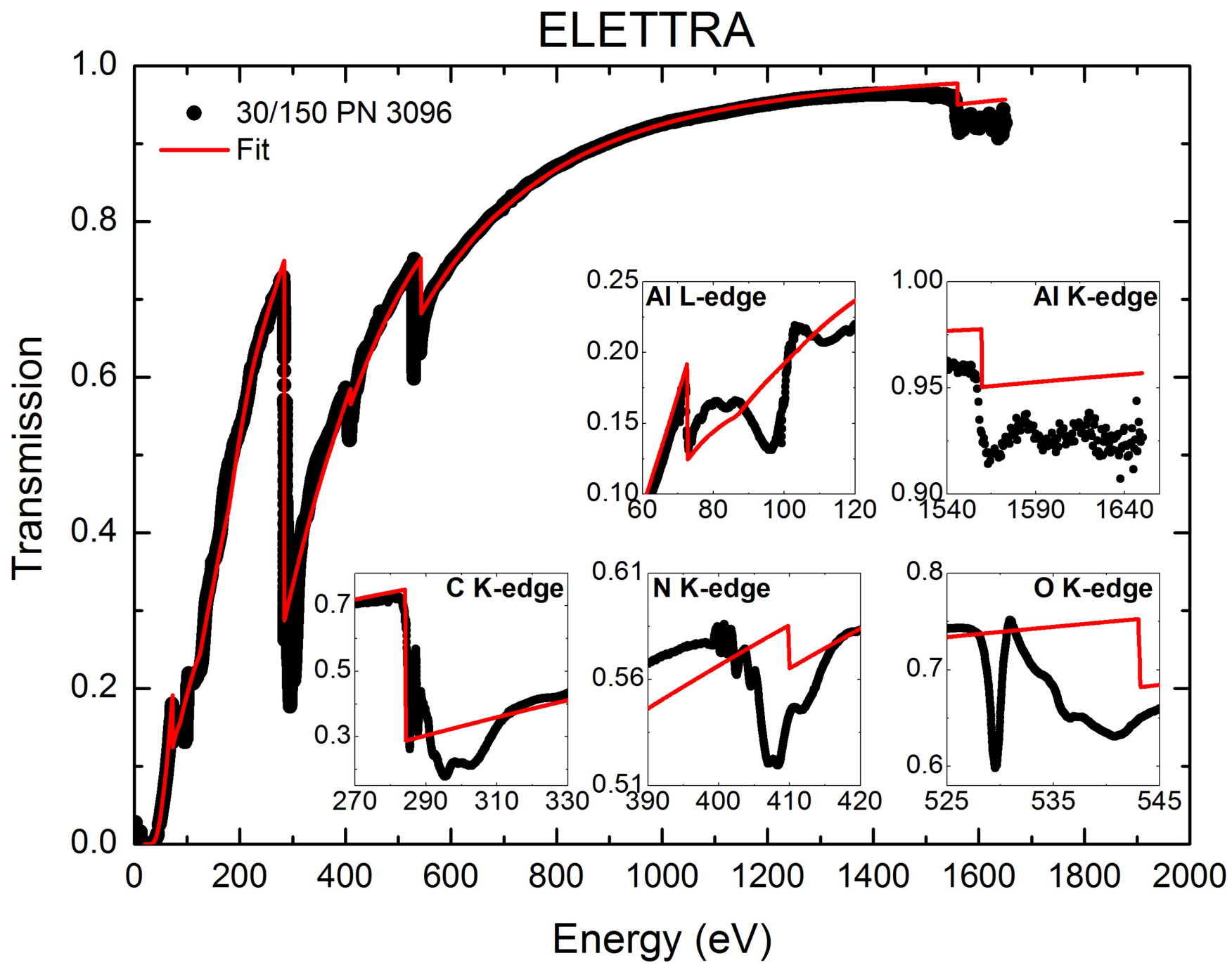
ELETTRA
30/150 PN 3096
Fit
Transmission
Energy (eV)
Al L-edge
Al K-edge
C K-edge
N K-edge
O K-edge

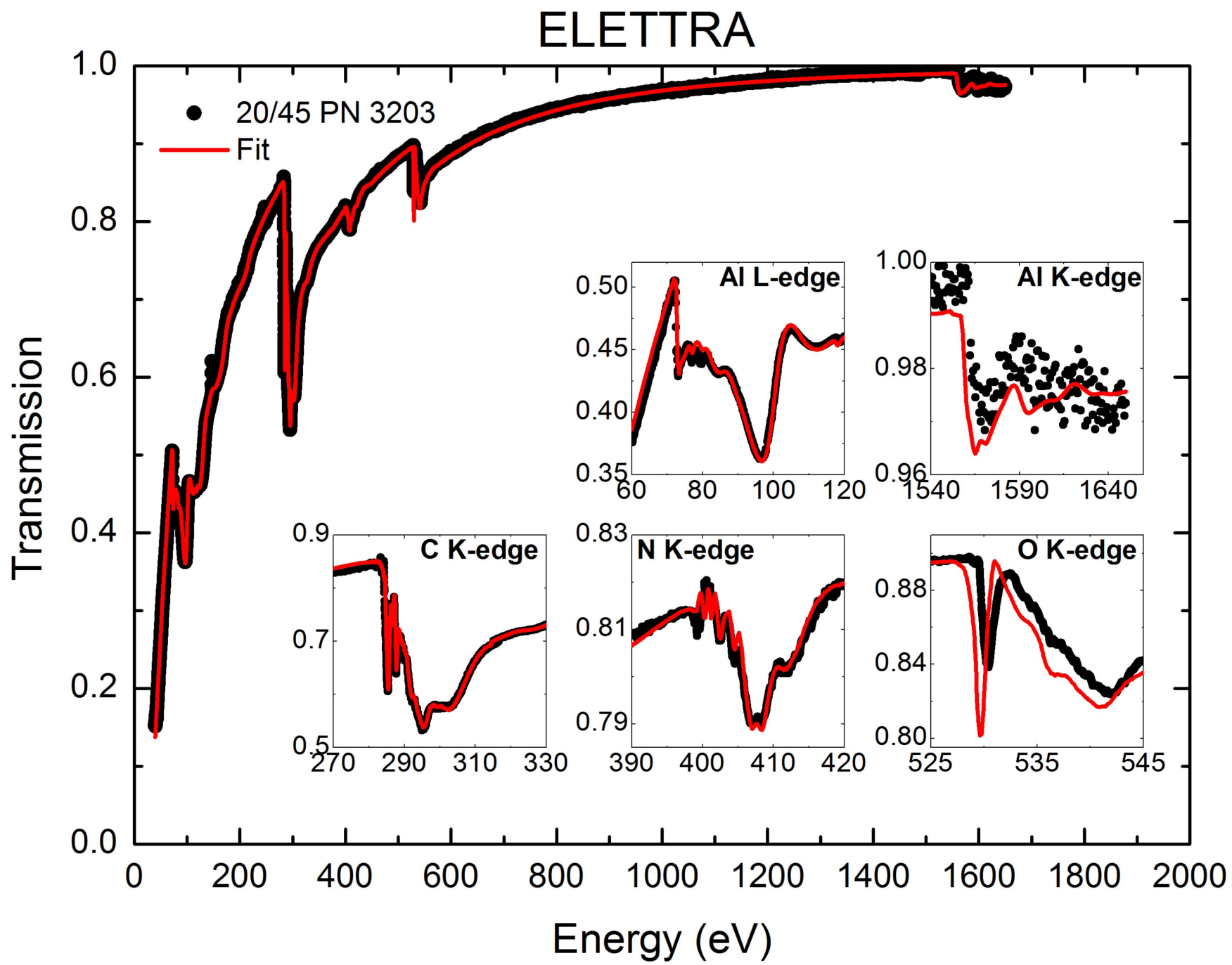
ELETTRA
20/45 PN 3203
Fit
Transmission
Energy (eV)
Al L-edge
Al K-edge
C K-edge
N K-edge
O K-edge

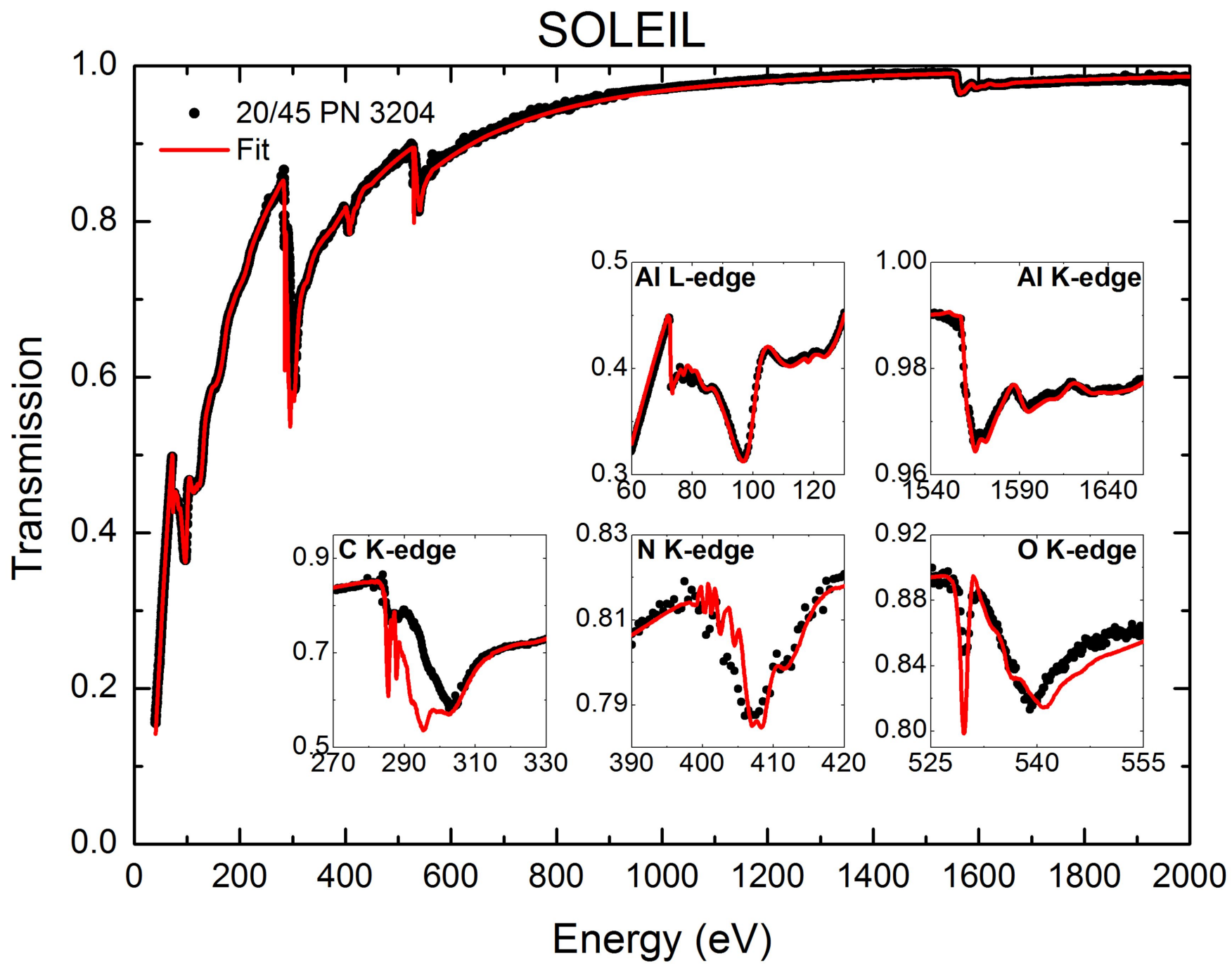
SOLEIL
20/45 PN 3204
Fit
Transmission
Energy (eV)
Al L-edge
Al K-edge
C K-edge
N K-edge
O K-edge

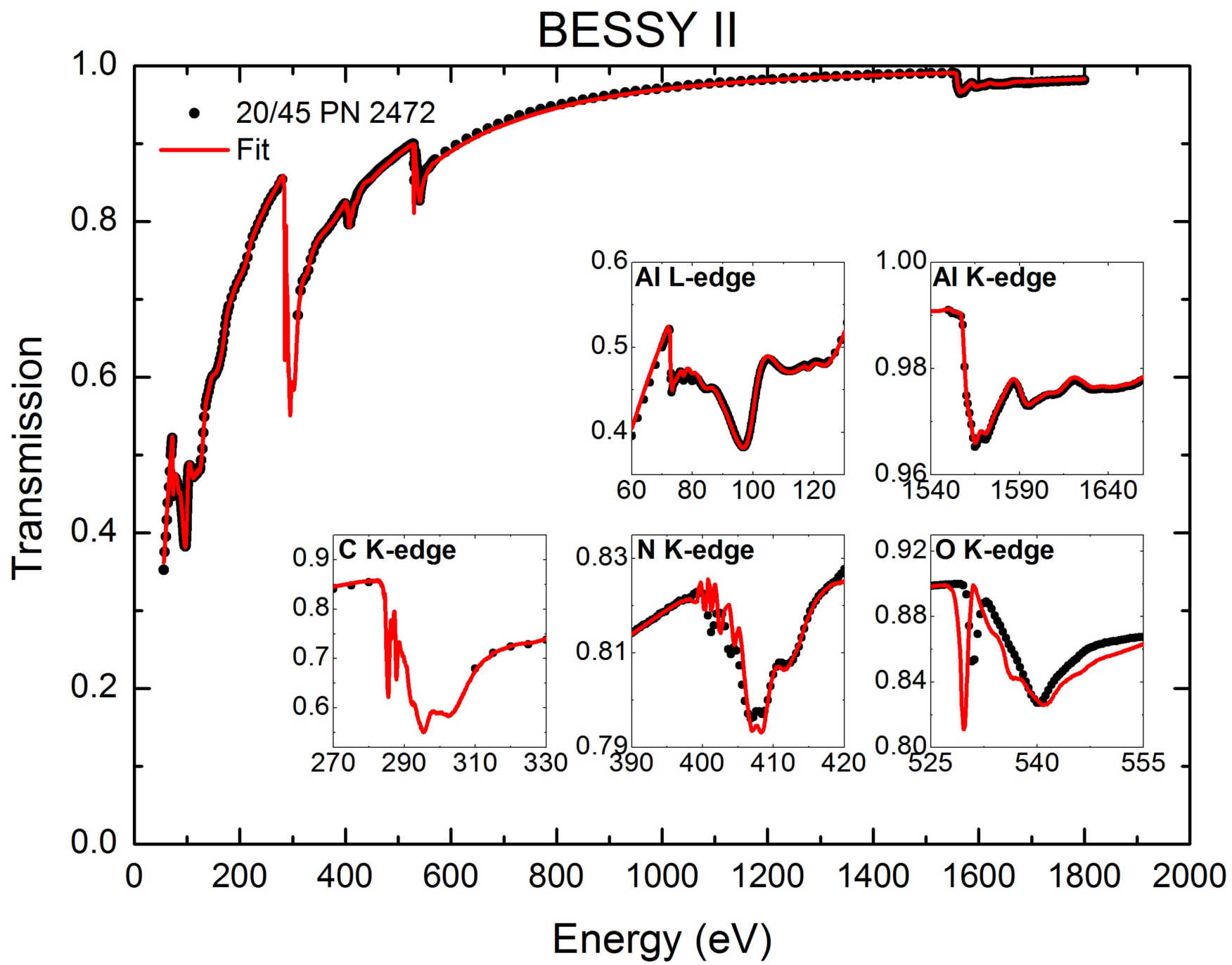
BESSY II
20/45 PN 2472
Fit
Transmission
Energy (eV)
Al L-edge
Al K-edge
C K-edge
N K-edge
O K-edge

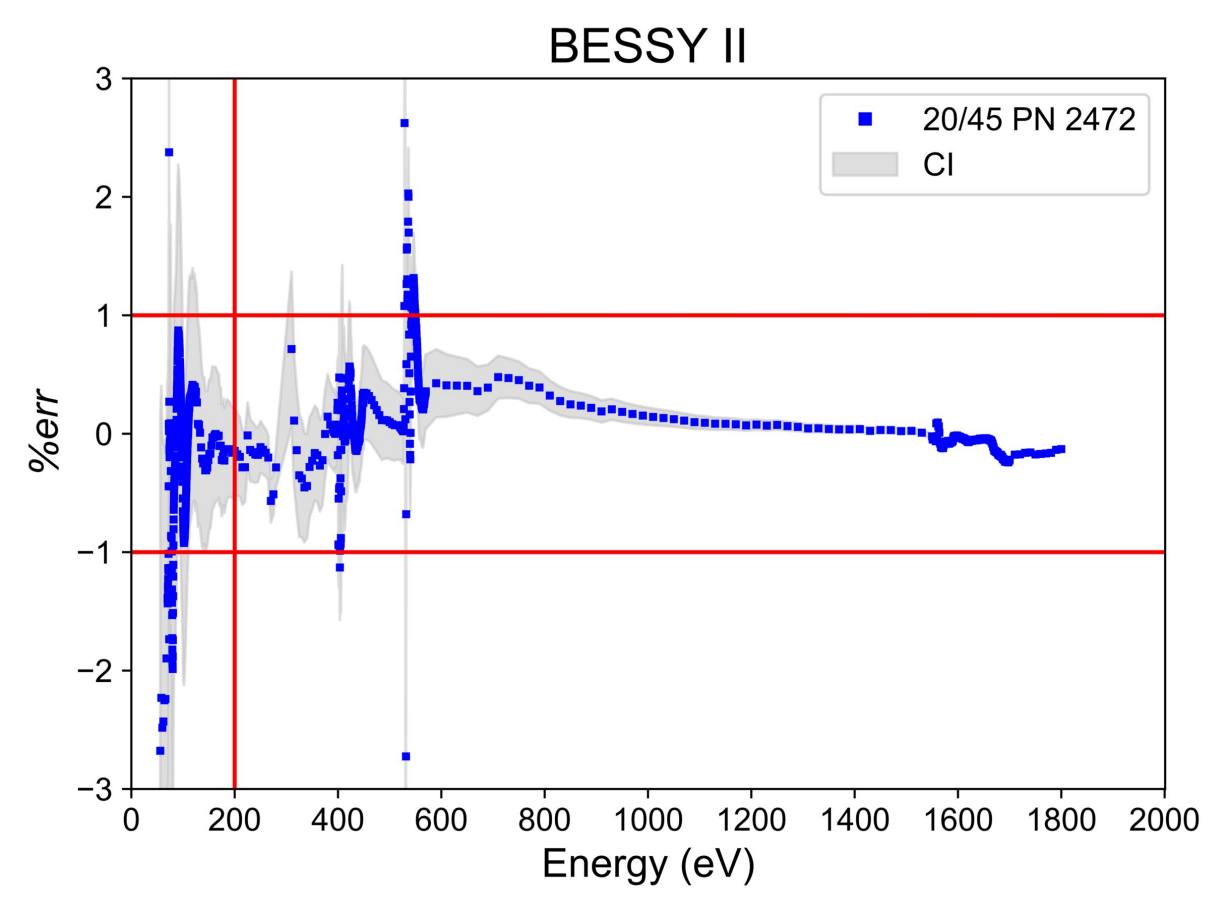
BESSY II
20/45 PN 2472
CI
%err
Energy (eV)
3
2
1
0
−1
−2
−3
0
200
400
600
800
1000
1200
1400
1600
1800
2000